NUMERICAL EVALUATION OF THE DILATOMETER TEST – AN IMPROVEMENT ON CORRELATIONS

Hao Shen[1] and Michael Jefferies[2]
[1] Klohn Crippen Berger, Brisbane, Australia. [2] Consulting Engineer, Vancouver, Canada

https://doi.org/10.56295/AGJ6044

ABSTRACT

A numerical approach is used to characterize the relationship between sand state and the normalized horizontal stress index K_D/K_0 from the Marchetti dilatometer test (DMT) to gain insight on extraction of geostatic stress conditions and soil stiffness from DMT data in sands. A 3D model of the DMT was implemented in Plaxis3D using the inbuilt NorSand model to simulate the DMT test, including both the insertion and subsequent expansion. The model was validated using DMT tests in Busan Sand, conducted using a calibration chamber, which were supported by extensive triaxial testing providing the soil properties. Provided that elastic shear rigidity I_r can be determined by means of geophysical method (readily done), the present investigation suggests numerical modelling of the DMT will be useful for characterizing in situ plastic modulus (which depends on soil fabric) as well as improving the understanding of geostatic stress by avoiding empirical correlations that neglect soil properties. The methodology developed is easily applied in engineering practice.

1 INTRODUCTION

Two large tailings dams, Fundao and Briumadinho, failed from conditions of zero excess pore pressure and with no evidence of prior distress causing enormous damage and many deaths. Understanding such failures requires knowing the state of stress in the dam, since it is the proximity of that state of stress to the soil's instability locus that indicates the safety – or otherwise - of the dam. However, the Brumadinho collapse was triggered by water pressures associated with geotechnical drilling (CIMNE, 2019) and that has led to reticence (prohibition ?) of using mud rotary boreholes – which effectively precludes pressuremeter testing that would be the usual investigation method for establishing insitu stresses. The Marchetti dilatometer (DMT) – a push in test - appears a useful method in such situations.

The dilatometer test (ASTM D6635) measures soil stress and stiffness using a pushed-in-place flat-plate probe. Two pressures are measured in a DMT test, the 'lift-off' pressure ('A') for the membrane to minimally move (0.05mm) and the pressure required ('B') to displace the membrane a standard distance (1.1 mm). The pressure p_0 (at zero displacement) is linearly back-extrapolated from the measured pressures A,B (Marchetti, 2001) with the horizontal stress index (K_D) being the normalised form of the contact pressure p_0:

$$K_D = (p_0 - u_0)/\sigma'_{v0} \tag{1}$$

…where u_0 is the hydrostatic pore pressure at the depth of testing and σ'_{v0} is the in situ effective overburden stress.

The DMT displaces soil during penetration and changes (generally increasing) the adjacent horizontal stress in the ground: $K_0 \neq K_D$. It is natural to invoke a critical state approach to understand the relation between K_0 and K_D, as such an approach automatically includes "compressibility" (= the slope of the critical state locus) and dilatancy (which depends on the void ratio offset from the soil's critical state, commonly called the state parameter ψ). Thus, Jamilkowski (1988) investigated the correlation between the dilatometer amplification factor K_D/K_0 and the state parameter ψ_0 and found:

$$K_D/K_0 = k_D \exp(-m_D \psi_0) \tag{2}$$

The challenge with evaluating the DMT thus becomes determining how k_d and m_d are related to the soil's properties (e.g. λ_{10}). Two approaches have been followed: correlations developed using calibration chambers and theoretically-based models.

Calibration chambers provide large uniform samples of known void ratio and with controlled stress states (in effect a large triaxial sample) into which the DMT is pushed; several such tests provide data to obtain the best fits of the coefficients k_D and m_D. The results of published calibration chamber studies are summarized in Table 1. It can also be observed from Table 1 that different testing campaigns on both Toyoura and Ticino sands produced different coefficients for the same sand – calibration chambers involve in the order of one tonne of sand and void ratio is difficult to determine

with precision. More generally, while it has been acknowledged that both k_D and m_D are soil-specific, a wide range of values apparent in Table 1 with a gap in the literature regarding how to quantify the effect of soil properties on k_D and m_D. Given how k_D and m_D vary among different sands from the calibration chamber results in Table 1, adopting an average ("universal") fit for any soil appears to be far from accurate. Yet, utilizing physical modelling methods, such as large calibration chambers, is typically time-consuming and likely inaccessible for smaller to medium-sized projects.

Table 1 The coefficients k_D and m_D from fitting calibration chamber results for various sands

Material	$\mathbf{k_D}$	$\mathbf{m_D}$	Source
Busan sand	2.405	4.54	Choi (2008)
Ticino sand	1.32	7.33	Lawter Jr and Borden (1990)
Ticino sand	1.3	8.08	Jamilkowski (1988)
Ticino sand	1.444	8.13	Choi (2008)
Cape Fear sand	2.74	2.31	Lawter Jr and Borden (1990)
Hokksund	1.19	8.63	Lawter Jr and Borden (1990)
Toyoura sand	1.05	3.07	Lawter Jr and Borden (1990)
Toyoura sand	3.676	3.06	Choi (2008)

In terms of theoretical correlations, much of the research has focused on modelling the DMT penetration in clays (Finno, 1993; Kouretzis et al., 2015; Yu et al., 1992) as the undrained (= constant volume) situation simplifies the analysis. Penetration of the DMT in sands has not been modelled theoretically.

This opens up an opportunity for numerical modelling to support in practical engineering applications. However, numerical simulation of penetration in sands is difficult – it is large-strain, with a frictional boundary, and with rotation of principal axes. Some recent progress has been obtained for penetration of the CPT using the Discrete Element Method (Arroyo et al., 2011), the Material Point Method (Martinelli and Pisanò, 2022), and Arbitrary Lagrangian-Eulerian (Monforte et al., 2017); but convincing matches to relevant calibration chamber data remain elusive. Thus, in the case of the CPT, penetration is commonly represented as spherical-cavity expansion with subsequent correlation to calibration chamber results – a procedure that allows direct assessment of how soil properties affect the CPT response (e.g. Shuttle & Jefferies, 1998).

The approach adopted in this paper follows this 'simplify but then calibrate' approach. The simplification is to treat penetration as a lateral displacement of the soil within a 3D finite element program by the equivalent of the DMT blade. The calibration is to compare the A, B pressures computed with those measured in a calibration chamber. Necessarily, the approach needs a data set containing sufficient triaxial tests to determine soil properties and DMT calibration chamber data on that sand. Such studies are rare. The tests on Busan sand were adopted as a complete dataset for our purpose.

A further consideration is the constitutive model. A 'standard' friction-dilation model ('Non-Associated Mohr Coulomb') is inadequate as the "elastic" properties are largely dominated by plastic strains and which then require invocation of 'strain dependent modulus' – there is no simple calibration. However, the last decade or so has seen critical state models (e.g. CASM, NorSand, SaniSand) providing good to very-good matches to measured sand behaviour. As such models are based on the state parameter, so are a natural starting point to investigate equation (1). Further, these critical state models have been implemented in geotechnical modelling platforms (e.g. Plaxis, Flac, RS2 and Sigma/W). We adopted Plaxis 3D and NorSand.

2 BUSAN SAND TESTS

2.1 BUSAN SAND

Busan sand is a natural sand dredged from the South Sea of Korea, and is poorly graded angular to subangular. The data used here is that reported by Choi (2008), digitizing from the paper record (there appear to be no digital records) and also over-laying computed trends on various published figures. The sand tested had a median grain size of 315 microns and negligible silt content, but did contain significant crushed shells reflecting its marine origin. A surprisingly large e_{min} = 0.658 was measured, although its specific gravity was a near common G_s= 2.62.

2.2 TRIAXIAL TESTS AND PROPERTIES

The properties were determined using twelve drained triaxial tests spanning a range of initial void ratios and confining stress; Figure 1 shows the state-paths of these tests. Two sample reconstitution methods were used, moist tamping for the looser samples and air pluviation for the denser (denoted as M and A respectively in the test naming).

The critical state locus (CSL) was assessed from the end state of the very loose tests and further influenced by behaviour found in the slightly denser samples as illustrated on Figure 1. This CSL with λ_{10}= 0.068 is slightly more compressible that usual for 'standard' quartz laboratory sands (where λ_{10}~0.05 is more common), but that is unsurprising given the known carbonate content of Busan sand.

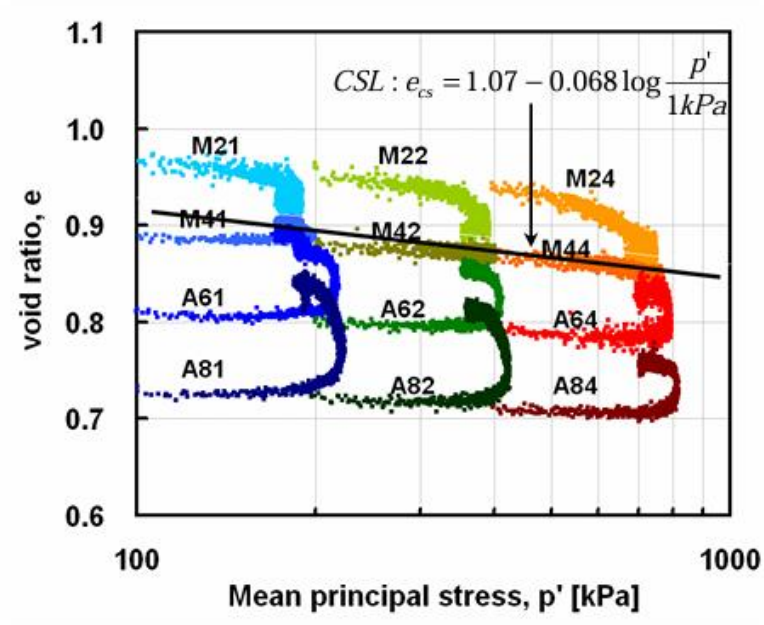

Figure 1: State paths of triaxial tests used to determine the properties of Busan sand (Choi, 2008)

The data on Busan sand as used here is taken from (Choi, 2008),. The original records were in the form of q vs e_a and e vs e_a. The void ratio trend data was fitted with the standard stress dilatancy for the triaxial test D, picking the limiting dilatancy D_{min} (the minimum because of the compression positive convention of soil mechanics) at the strain of peak strength (and which itself is presented as the stress-ratio η_{max}). The results are shown on Figure 2a, and are nicely fitted by the Taylor-Bishop 'interlocking' strength model (the trendline shown on the figure):

$$\eta_{max} = M_{tc} - (1 - N)D_{min} \quad (3)$$

…where M_{tc} is the stress ratio η in the critical state and N is Nova's (1982) volumetric coupling parameter. The meaning of these properties is illustrated on the figure and the calibrated values for Busan sand were M_{tc} =1.44 and N=0.58; both values are significantly larger than found with 'standard' laboratory quartz sands, implying that the DMT calibration will also be unusual.

The corresponding state-dilatancy behaviour shown in Figure 2b is fitted with the usual relation:

$$D_{min} = X_{tc}\, \psi_{Dmin} \quad (4)$$

…where X_{tc} = 3.6 is the state-dilatancy coefficient, and whose value is 'not unusual' for poorly graded sands. Note that the state parameter in equation (4) is the value at the occurrence of D_{min}, not the value at the start of the test; further the trend line passing through the plot origin is a theoretical requirement.

2.3 KOREAN CALIBRATION CHAMBER

The Korea University Calibration Chamber System (KUCCS) comprises a calibration chamber 1.2m diameter and 1.0m high with servo-controlled operation to consolidate soil specimens at a variety of stress paths including K_0 (zero lateral strain). Samples were prepared by an enhanced air-pluviation method to provide a uniform density of the test sample. The distinctive feature of the pluviation system was using a porous plate to minimize the effect of drop distance and to control the drop height without changing the deposition intensity.

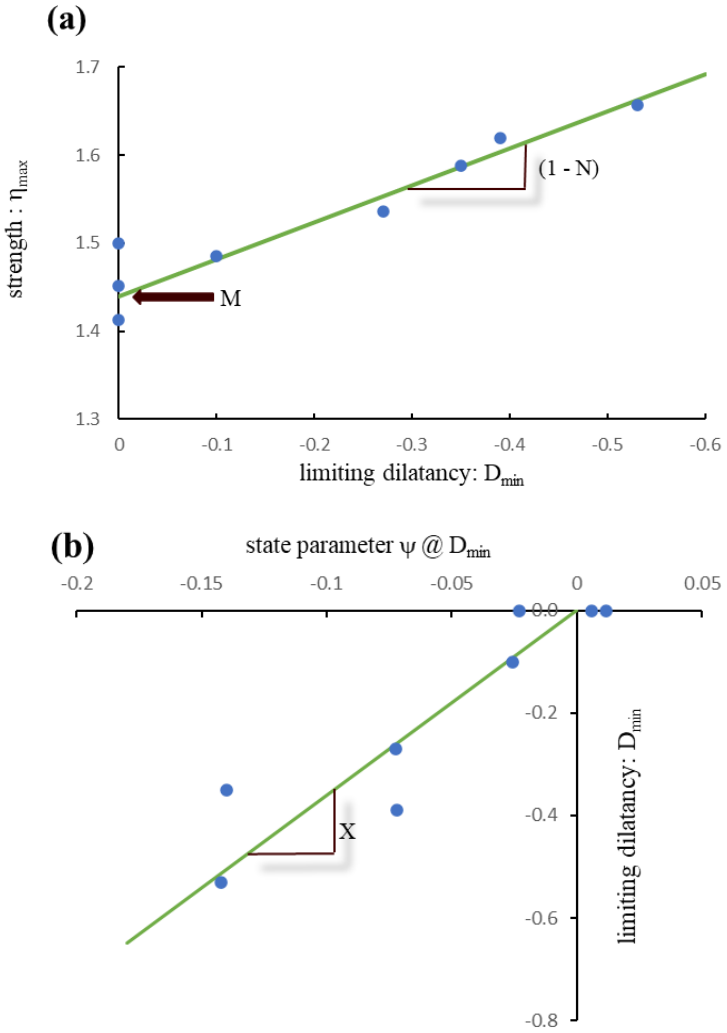

Figure 2: Properties of Busan sand in triaxial compression

2.4 ELASTICITY

The calibration chamber contained 'bender elements' for measuring the seismic shear wave velocity in the usual way. Both horizontal and vertical ray used, and G_{max} was measured during each test. We used an average of the two paths, and converted this to G_{max}. As usual, there was a strong effect of stress level and void ratio on G_{max}. We used the three-parameter elastic model:

$$G_{max} = \frac{A}{e - e_{min}} \left(\frac{\bar{p}}{1\ kPa}\right)^{n_G} \quad (5)$$

…where A is a coefficient (normally in MPa, the same units as G_{max}), n_G is an exponent on the normalized mean confining stress, and e_{min} is a third soil property that reflects the void ratio when the 'sand' transitions to 'sandstone'. All three properties were determined by simultaneous regression to minimize error between (7) and 'ground truth': Figure 3. Data was within 5% of (6), and unbiased, using the properties: A = 2.95 MPa, n_G=0.5 and e_{min} = 0.45.

2.5 DMT CALIBRATION

After applying the horizontal and vertical stress to the sample in the chamber, the DMT was pushed into the sample on the central axis. DMT tests were performed in the central depth region to avoid effects of the top and bottom boundaries of the chambers (aspects readily seen on the continuous record of a CPT that were also carried out). The DMT tests were done in the standard manner, and were performed at four vertical effective stress states and three sand densities. Both normally consolidated and over-consolidated cases were tested. The test data reduces to the expected form of horizontal stress amplification factor with ψ of equation (2), with the same trend for over-consolidated and normally consolidated samples, as illustrated on Figure 4.

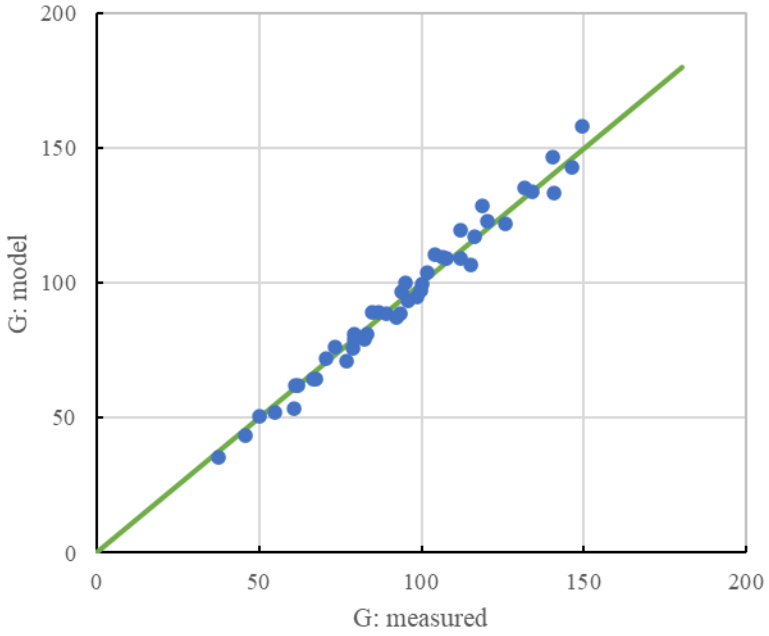

Figure 3: Comparison of elastic idealization with ground truth

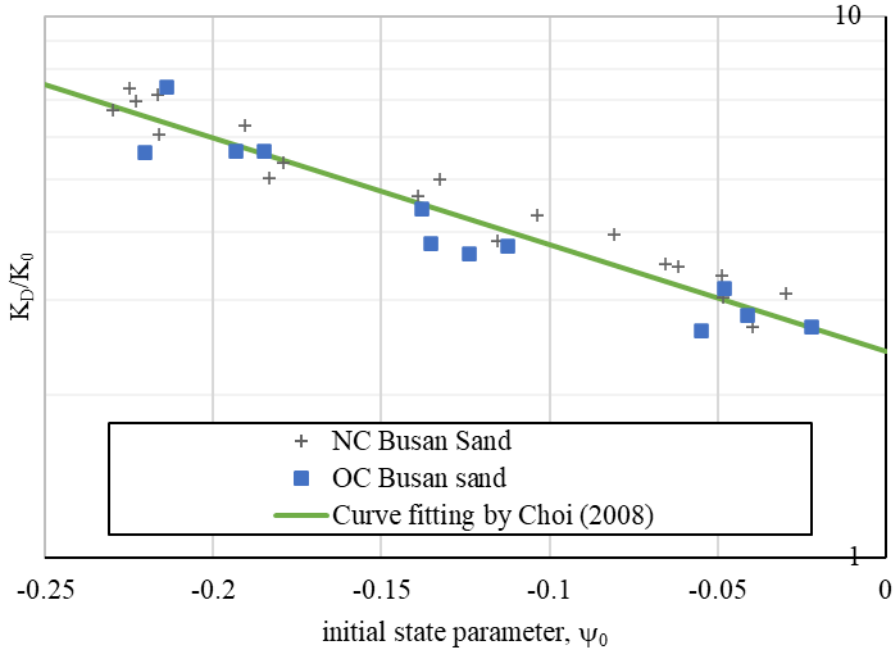

Figure 4: DMT horizontal stress amplification in Busan Sand chamber tests (Choi, 2008)

3 NUMERICAL MODEL FOR DMT

3.1 CONSTITUTIVE IDEALIZATION

Critical state theory combines soil properties – which are independent of void ratio or confining stress and in principle measurable on reconstituted samples – with 'state measures' that reflect the insitu condition of the soil and which may also show natural variability. Common state measures are the state parameter ψ (essentially controlling limiting dilatancy), over-consolidation ratio (which reflects 'structure' as well as geologic history and thus the onset of yielding), and the elastic shear modulus G_{max} (treated as a state measure because of dependence on the arrangement of soil particle contracts).

The critical state model NorSand (NS; Jefferies, 1993) was used as implemented in Plaxis3D (Bentley, 2023) and which includes the updates discussed in Shuttle & Jefferies (2016). NS includes all three state measures and the five soil properties discussed earlier: Γ, λ describe the critical state locus; M, N describe stress-dilatancy; χ describes state-dilatancy. There is one NS-specific property, the plastic hardening modulus H that describes the plastic stiffness (and which is strongly correlated to the inverse of λ). Soil properties are determined in triaxial compression and are largely familiar.

Iterative modelling is used to determine H, initially assuming a constant value for any test and then refining for the typical trend: $H = H_0 + H_\psi \psi$. Examples of the achieved calibration to four tests of different initial void ratio are shown on Figure 5; there are close fits of NS to data before peak strength, with post-peak diverging because of localization where the reported test σ–ε does not capture the sand behaviour in the localizing shear-band. The calibrated trend for H is shown on Figure 6, where the trend has been weighted to the air-pluviated samples as having the same 'fabric' as the sand placed in the calibration chamber.

The soil properties used in our simulations of the calibration chambers tests on the DMT in Busan Sand are summarized on Table 2.

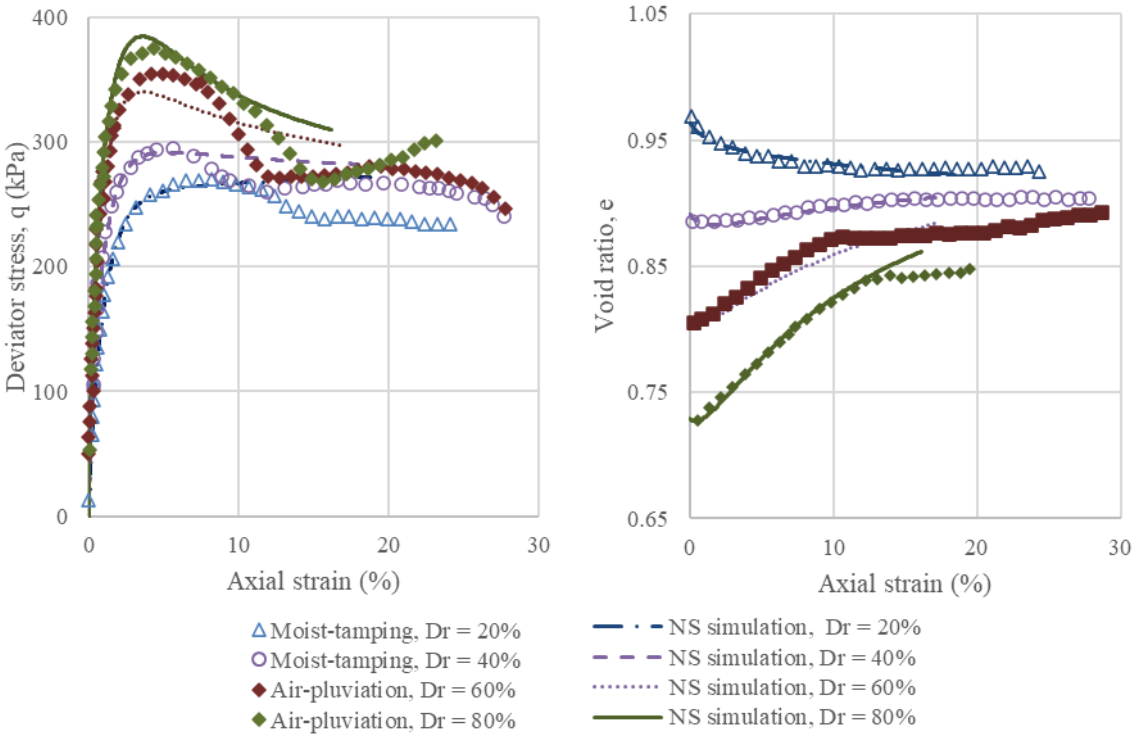

Figure 5: Achieved fits (lines) to triaxial compression data (digitized from paper record) of Busan Sand (Choi, 2008) (D_r% are initial relative densities of the sample; these tests at p_0=100 kPa)

Table 2 NorSand parameters for Busan Sand

Soil	λ_e	Γ	M_{tc}	G_{ref} (MPa)	n_G	H_ψ	H_0	N	χ_{tc}
Busan Sands	0.0295	1.07	1.44	2.95	0.5	800	90	0.55	3.6

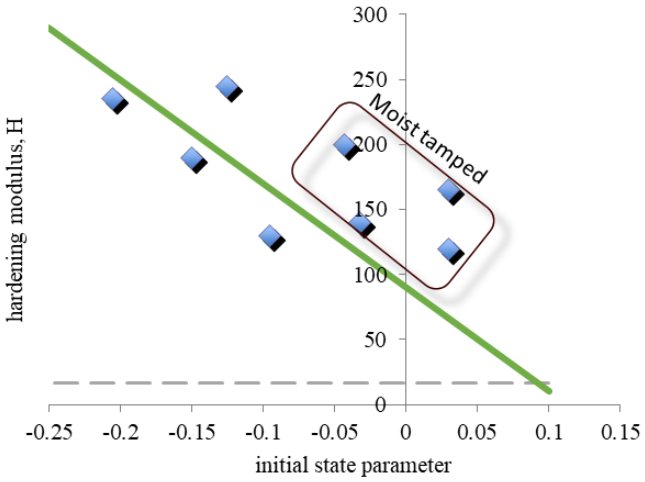

Figure 6: Calibrated trend for plastic hardening modulus

3.2 GEOMETRIC IDEALIZATION

The shape of the flat dilatometer blade (95 mm width, 15 mm thick, and the tapered section of 50 mm long) requires simulating DMT penetration as a 3D problem to accurately consider the increase in horizontal soil stresses near the membrane because of soil displacement during blade penetration; however, the symmetry of the flat blade along its midplane allows simulating only a portion equivalent to half of the flat blade's thickness, specifically aimed at displacing the central soil elements. The subsequent expansion of the DMT membrane further reinforces the requirement that the DMT test shall be treated as 3D.

3.3 INSERTION OF DMT

The insertion of the DMT was approximated by displacing the mesh horizontally such that the physical size of the DMT would then fit. This approximation does not account for the large shear strains experienced by the soil that was initially below the axis of the DMT which, as understood by a cavity-expansion analogue, would have evolved to its critical void ratio regardless of initial conditions. The approximation used does not include a layer of soil in its critical state adjacent to the DMT blade.

In terms of boundary condition, a fixed displacement along the X axis, perpendicular to the blade and just beneath the blade tip, is implemented as shown in Figure 7. This method resolves issues that would arise if a stress boundary were applied; such conditions would cause soil nodes to shift outward, disrupting symmetry boundary conditions and complicating numerical convergence. Along the Y axis adjacent to the DMT blade, a constant horizontal stress is maintained, ensuring a smooth transition of displacement rather than an abrupt jump that could distort the elements. For the rest of the displaced soil block, the bottom nodes are completely fixed, while constant stress is maintained on all other surfaces.

The mesh dimensions (2m by 2m by 1m for X, Y, and Z axes respectively, as shown in Figure 8, were optimized through trial and error to mitigate boundary effects on the analysis outcomes. The model's width along the X-axis, perpendicular to the blade, is approximately 267 times the blade's half-thickness (7.5 mm). While ensuring the model is sufficiently large is crucial to reduce boundary effects, refining the mesh near the blade's tapered section and around the membrane is equally important. This localized refinement, as shown in Figure 8, ensures that pressure measurements on the membrane are precise and helps in preventing issues with simulation convergence.

3.4 TEST IMPLEMENTATION

To model the expansion of the circumferentially fixed 60 mm diameter steel flexible membrane used in the DMT, we employed a series of 11 annuli to define the surface areas of the mesh. Displacements were prescribed based on an ideally expanding spherical cap that conforms to the 60 mm diameter membrane, varying from zero at the circumference to a maximum of 1.1 mm at the centre, as illustrated in Figure 8-b. The horizontal effective stresses on the DMT membrane area were extracted from Gauss stress points within the finite element mesh and averaged to obtain the DMT pressure measurements. This paper focuses on the contact pressure p_0, which is central to interpreting geostatic stress from the DMT.

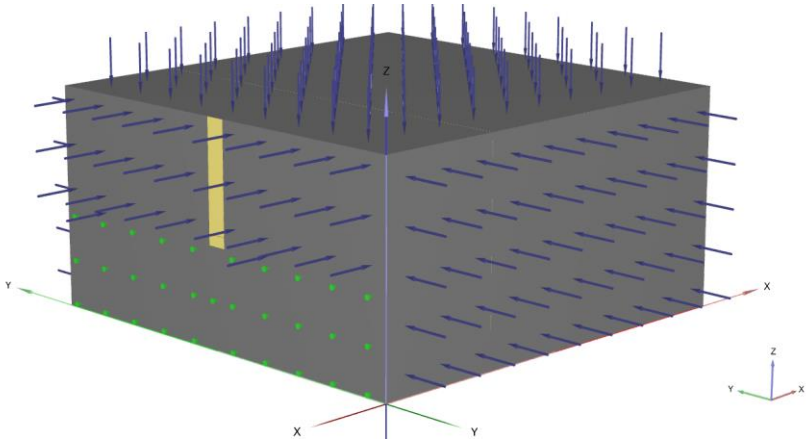

Figure 7: The deformation and stress boundary of the FEM model in Plaxis 3D

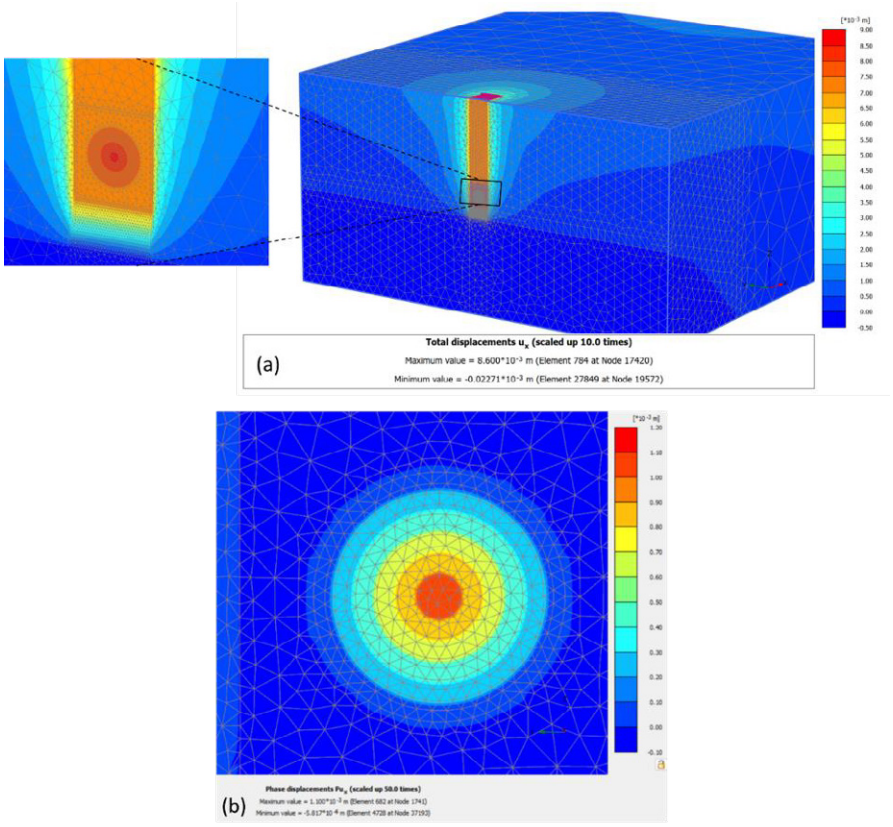

Figure 8: The FEM mesh used for analysis: (a) total horizontal displacement, (b) horizontal displacement during membrane expansion

4 VALIDATION

4.1 SIMULATIONS PROGRAMME

The DMT tests conducted in the KUCCS involved vertical loads of 50 kPa, 100 kPa, 200 kPa, and 400 kPa for normal consolidation conditions, followed by unloading at the same intervals for over-consolidation conditions. The initial void ratios of the samples were 40%, 60%, and 80% in terms of relative density, which correspond to a range of state parameters of $-0.23 < \psi_0 < -0.02$ (see Figure 4).

To cover representative ranges of void ratios tested, the simulation program included initial state parameters (ψ_0) of -0.2, -0.15, -0.1, and -0.05. As such, a total of 48 simulations were carried out in Plaxis3D (Version 2023.2.2.1059) for validation with these scenarios being summarized on Table 3. The NorSand implementation in Plaxis employs a two-parameter model for elasticity (Benteley, 2023):

$$G_{max} = G_{ref}\left(\frac{\bar{p}}{p_{ref}}\right)^{n_G} \tag{6}$$

…where G_{ref} is shear modulus in MPa at the reference at the reference pressure p_{ref} equal to 100 kPa (a convention), n_G is an exponent on the normalized mean confining stress which is the same as that in equation (5). As a result, the three-parameter elastic idealization that includes the void ratio in equation (5) was decomposed into three sets of three two-parameter elastic idealization in equation (6) to represent respective sets of void ratios. The resulting trends are illustrated in Figure 9.

Table 3: Modelling conditions of the simulation programme

G_{ref} (MPa) at = 100 kPa	n_G	OCR	K_0	σ_v	I_r = G/p
66, 83, 100	0.5	1.0	0.4	50, 100,200,400	426, 536, 602, 645, 758, 852, 913, 1072, 1205, 1291, 1515, 1826

Note: The three G_{ref} represents the sands at relative densities of 40%, 60%, and 80%, respectively.

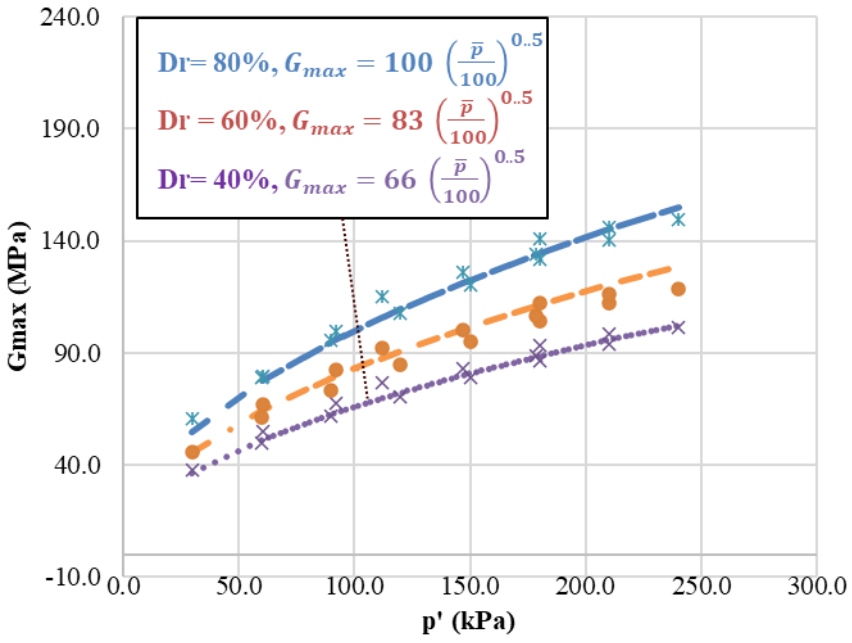

Figure 9: The two-parameter elastic idealization adopted in Plaxis 3D

4.2 SIMULATION RESULTS AND THE CORRECTIONS

Following each simulation, horizontal effective stress on the DMT membrane was extracted from Gauss stress points and averaged to obtain the contact pressure p_0. Then p_0 was normalized by means of equation (2) to obtain K_D. Figure 10 gives an example simulation showing how the contact pressure evolved during the simulated insertion of the DMT blade – a rather stiff initial response softened quickly (within 2mm) into a quasi-linear trend to p_0. During the subsequent membrane expansion, the pressure measurements become approximately linear.

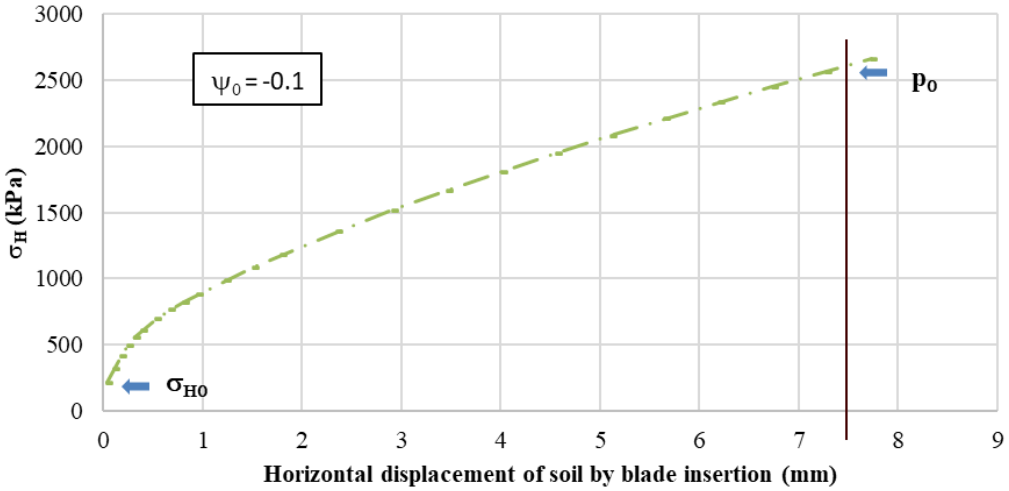

Figure 10: Example of computed evolution of contact pressure during DMT insertion

Using the soil properties presented in Table 2 and the initial states in Table 3, simulations were performed to compare with the DMT calibration chamber (CC) data from Choi (2008). While keeping the other NorSand properties constant, the DMT simulations varied only in their initial states, including initial mean effective stresses p_o, elastic shear rigidity I_r, and initial state parameter ψ_0. This allowed the creation of trend lines between the simulated normalized dilatometer horizontal index K_D/K_0 and initial state parameter ψ_0. Figure 11 presents the relationship between the fitted trend lines and the CC data.

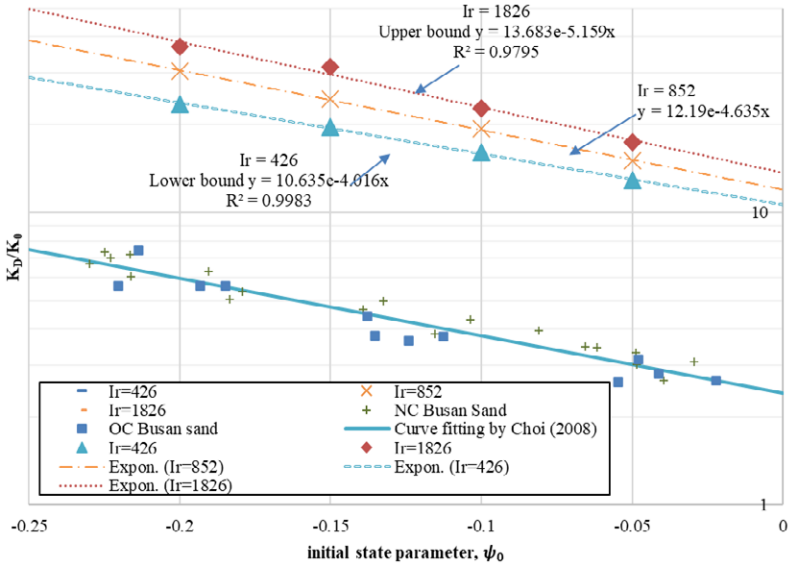

Figure 11: Comparison of numerical results for blade cavity expansion in Busan sand with data from calibration chamber test

While I_r was not considered by Choi (2008), the DMT simulations in this paper varied the trend lines according to different I_r values. The simulated K_D/K_0 results are consistently higher than the K_D/K_0 results observed in CC. This difference is not unexpected given the more stringent boundary conditions of the proposed numerical model. Similar to the universal shape function used for cavity expansion and CC normalised tip resistances in the CPT tests (Ghafghazi and Shuttle, 2008; Shuttle and Jefferies, 2016, 1998), a shape function is also necessary for the DMT tests.

The DMT shape function would compensate for aspects of the DMT sounding not captured by the numerical model. Penetration of the DMT involves friction on the blade surface similar to that measured with the CPT but we have not included that boundary condition. More seriously, the implemented model of the DMT is that for an infinitely long blade above the sensing element to simplify the geometry and avoid mesh dependency issues. In reality, as illustrated on Figure 12, the cross-section of the blade (14.3 cm^2) changes to that of the push rod (often CPT rods of 10 cm^2 cross-section) which allows soil to relax back – and, as can be observed in Figure 12 the distance of this relaxation area from the sensing element is comparable to the size of that element. The shape function is thus proposed to address these differences between the numerical blade cavity expansion and the actual blade penetration.

Figure 12: View of DMT highlighting void space in close proximity to sensor

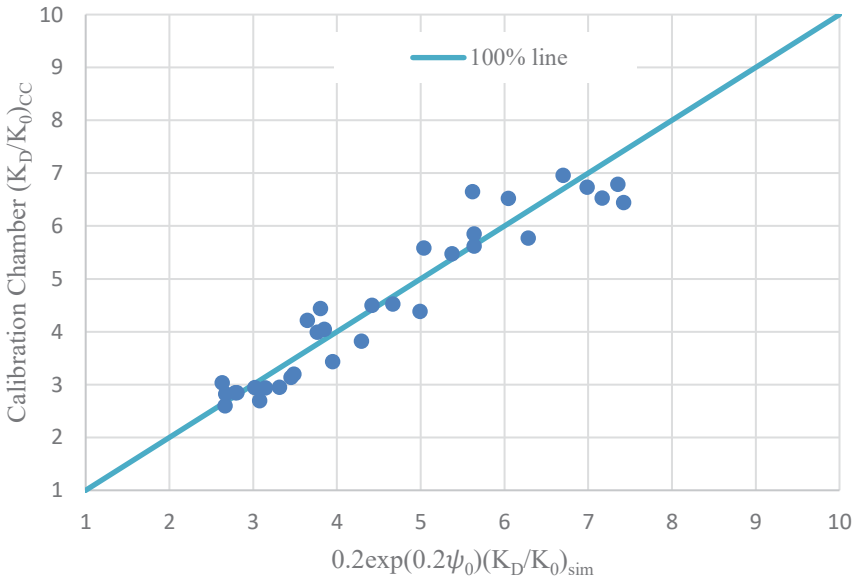

Figure 13: Simulated K_D/K_0 scaled by a shape function against K_D/K_0 in CC for Busan sands

The numerical results scale to those in the calibration chamber as:

$$(K_D/K_0)_{CC} = 0.2exp\ (0.2\psi_0)(K_D/K_0)_{sim} \tag{7}$$

…with Figure 13 comparing the simulated K_D/K_0 results, scaled by equation (7), to K_D/K_0 in CC for Busan sands. This comparison yields a Pearson correlation coefficient of 0.96 and a mean absolute error of approximately 0.29, independent of the initial state parameter (ψ_0), stress level, or elastic shear rigidity I_r.

5 USING THE PROPOSED METHODOLOGY

This study presents a numerical approach to quantify the relationship between the dilatometer amplification factor K_D/K_0 and the initial state parameter ψ_0 in sands. The method offers a framework for interpreting geostatic stress conditions and soil stiffness from DMT data. Since the proximity of the in-situ stress state to the soil's instability locus is a key indicator of tailings dam safety, the proposed approach holds significant practical importance.

However, the method has been developed based on a unique dataset —possibly the only one of its kind available in the published literature— that includes both extensive triaxial testing and calibration chamber results, which presents a limitation in terms of generalizability. In contrast, state parameter interpretation using the CPT—such as through the CPTwidget (Shuttle, D., 2019)—is more established, drawing upon a much broader and more diverse database of sands.

To apply the proposed methodology in practice, the following steps are recommended:

1. **Laboratory Testing:**
   Conduct both consolidated undrained and consolidated drained triaxial compression tests to define the critical state line, as well as to determine stress–dilatancy and state–dilatancy parameters. Accompany these with index tests including particle size distribution, specific gravity, and maximum and minimum index densities.
2. **In-situ Testing:**
   Perform DMT and CPT tests side-by-side, and obtain in-situ shear wave velocity measurements from either test as feasible.

Using the recovered state parameter from CPT data, such as that obtained via CPTwidget, the in-situ K_0 may be estimated.

Future research would benefit from additional datasets that include DMT results obtained from calibration chamber testing, alongside comprehensive laboratory testing, to further validate and refine the methodology.

6 CONCLUSION

(1) This study underscores the soil-specific nature of the relationship between K_D/K_0 and ψ_0. A gap is identified in the literature concerning the quantification of soil properties' effects on this relationship. Therefore, numerical modelling approach emerges as a viable and effective approach to bridging this gap for interpreting the DMT results across different soil types in practise, provided an appropriate soil model is used.

(2) The recent tests on the DMT in Busan Sand, conducted using a calibration chamber, offer valuable validation cases. This DMT data is supplemented by extensive triaxial testing to accurately determine the sand's properties. These tests are interpreted in the NorSand (NS) soil model, ensuring the analysis is based on well-characterized soil properties.

(3) Finite element models using Plaxis 3D, with updated Lagrangian formulation enabled, are created to simulate the DMT blade insertion process by displacing half of the flat blade's thickness and its taper tip section of the soil elements. This idealization allows for a straightforward setup of the numerical model, which can be practically repeated with different NS parameters to investigate the DMT responses. With a shape function that compensates for aspects of the DMT sounding not captured by the numerical model, the estimated K_D/K_0 to ψ_0 trends fall well within the range of results observed in normally consolidated Busan sands within the calibration chamber.

CRediT authorship contribution statement

Hao Shen: Conceptualization, Formal analysis, Writing - original draft. **Michael Jefferies**: Conceptualisation, Formal analysis, Writing – original draft, Writing - review and editing.

7 REFERENCES

Benteley, 2023. User Defined Soil Models - NorSand: An elasto-plastic model for soil behaviour with static liquefaction.

Choi, S.K., 2008. Estimation of Stress History of Sands using CPT and DMT (PhD). Korea University.

Finno, R., 1993. Analytical interpretation of dilatometer penetration through saturated cohesive soils. Geotechnique 43, 241–254. https://doi.org/10.1680/geot.1993.43.2.241

Ghafghazi, M., Shuttle, D., 2008. Interpretation of sand state from cone penetration resistance. Géotechnique 58, 623–634. https://doi.org/10.1680/geot.2008.58.8.623

Jamilkowski, M., 1988. New correlations of penetration tests for design practice. Proc ISOPT- Orlando Fla 263–296.

Jefferies, M., 1993. Nor-Sand: a simple critical state model for sand. Géotechnique 43, 91–103. https://doi.org/10.1680/geot.1993.43.1.91

Jefferies, M., Been, K., 2016. Soil Liquefaction: A Critical State Approach.

Kouretzis, G.P., Ansari, Y., Pineda, J., Kelly, R., Sheng, D., 2015. Numerical evaluation of clay disturbance during blade penetration in the flat dilatometer test. Géotechnique Lett. 5, 91–95. https://doi.org/10.1680/jgele.15.00026

Lawter Jr, R.S., Borden, R.H., 1990. Determination of Horizontal Stress in Normally Consolidated Sands by Using the Dilatometer Test: A Calibration Chamber Study. Transp. Res. Rec.

Marchetti, S., 2001. The Flat Dilatometer Test (DMT) in Soil Investigations, TC16. International Society for Soil Mechanics and Geotechnical Engineering (ISSMGE). https://doi.org/10.1007/978-3-319-73568-9_174

Marchetti, S., 1980. In situ tests by flat dilatometer. J. Geotech. Eng. Div. 106, 299–321. https://doi.org/10.1061/AJGEB6.0000934

Martinelli, M., Pisanò, F., 2022. Relating cone penetration resistance to sand state using the material point method. Géotechnique Lett. 12, 131–138. https://doi.org/10.1680/jgele.21.00145

Monforte, L., Carbonell, J.M., Arroyo, M., Gens, A., 2017. Performance of mixed formulations for the particle finite element method in soil mechanics problems. Comput. Part. Mech. 4, 269–284. https://doi.org/10.1007/s40571-016-0145-0

Shen, H., Haegeman, W., Peiffer, H., 2018. Design, Use, and Interpretation of an Instrumented Flat Dilatometer Test. Geotech. Test. J. 41, 247–262. https://doi.org/10.1520/GTJ20170090

Shuttle, D., 2019. CPTwidget: a finite element program for soil-specific calibration of the CPT.

Shuttle, D., Jefferies, M., 2016. Determining silt state from CPTu. Geotech. Res. 3, 90–118. https://doi.org/10.1680/jgere.16.00008

Shuttle, D., Jefferies, M., 1998. Dimensionless and unbiased CPT interpretation in sand. Int. J. Numer. Anal. Methods Geomech. 22, 351–391. https://doi.org/10.1002/(SICI)1096-9853(199805)22:5<351::AID-NAG921>3.0.CO;2-8

Yu, H., Carter, J., Booker, J., 1992. Analysis of the dilatometer test in undrained clay. Presented at the Predictive soil mechanics: Proceedings of the Wroth Memorial Symposium held at St Catherine's College, Oxford, 27-29 July 1992, Thomas Telford Publishing, pp. 783–795.

Notation

Subscripts

c	Critical state
0	Initial condition
1, 2 ,3	Principal directions of stress or strain
ref	Reference stress level; by convention, p_{ref} = 100 kPa
tc	Triaxial compression condition

Superscripts

e	Elastic
p	Plastic

Dimensions

F	force
L	length

Stress Variables (all stress as 'effective')

$\sigma_{1, 2, 3}$	[FL^{-2}]	Principal stresses
σ_m	[FL^{-2}]	Mean effective stress
σ_q	[FL^{-2}]	Deviatoric stress invariant
η	[-]	Dimensionless distortional stress measure h = s_q / s_m

Strain Variables

$\varepsilon_{1, 2, 3}$	[-]	Principal strains (assumed coaxial with principal stresses)
ε_v	[-]	Volumetric strain $e_v = e_1 + e_2 + e_3$
ε_q	[-]	Distortional strain measure work conjugate with s_q
D	[-]	Dilatancy, as ratio of strain rates de_v/de_q
D^p	[-]	Plastic dilatancy, as ratio of strain rates de_v^p/de_q^p

State Variables

e	[-]	Void ratio
ψ	[-]	State parameter, ψ = e - e_c

Critical State & Soil Properties

Γ	[-]	Reference void ratio on CSL, defined at p′ = 1 kPa
λ	[-]	Slope of CSL in e-ln(s_m) space for semi-log idealization
λ_{10}	[-]	Slope of CSL, but defined on base 10 logarithms (= 2.3 l)
M	[-]	Critical friction ratio, equals η_c at the critical state.
N	[-]	Nova's volumetric coupling coefficient in stress-dilatancy
χ	[-]	State dilatancy coefficient (soil property)
E, G	[FL^{-2}]	Respectively, Young's modulus and elastic shear modulus
ν	[-]	Poisson's ratio
I_r	[-]	Elastic shear rigidity
H	[-]	Plastic hardening modulus

DMT indexes

A, B	[FL^{-2}]	Respectively, the DMT measured pressures at central membrane displacements of 0.05 mm and 1.1 mm
ΔA, ΔB	[FL^{-2}]	Respectively, the DMT membrane stiffness corrections at central membrane displacements of 0.05 mm and 1.1 mm
Z_M	[FL^{-2}]	The DMT gage reading when vented to atmosphere
K_D	[-]	The DMT horizontal stress index
k_D, m_D	[-]	dimensionless coefficients in $K_D/K_0 = k_D \exp(-m_D \psi_0)$

The horizontal stress cone coefficients

a, b	[-]	dimensionless coefficients in $\sigma'_{hc}/\sigma'_{h0} = a \exp(b\psi_0)$